

A Lightweight Method for Constructing a Global Digital Elevation and Terrain Database

Bo Zhao,^{1,2} Jiayu Wang,^{3*} Yongqiang Wei,^{4,5} and Hui Xia³

¹College of Earth and Environmental Sciences, Lanzhou University, Lanzhou 730060, China

²Surveying and Mapping Institute of Gansu Provincial Bureau of Geology and Mineral Resources, Lanzhou 730060, China

³Changjiang Spatial Information Technology Engineering Co., Ltd. (Wuhan), Wuhan 430010, China

⁴Xi'an Research Institute of Surveying and Mapping, Xi'an 710054, China

⁵State Key Laboratory of Geo-information Engineering, Xi'an 710054, China

(Received August 26, 2024; accepted November 28, 2024)

Keywords: database, digital elevation model (DEM), digital relief model (DRM), spaceborne laser altimetry satellite

We propose a lightweight method for constructing a global digital elevation and terrain database in consideration of the satellite flight path. First, a global maximum/minimum elevation database with a grid size of $0.05^\circ \times 0.05^\circ$ was generated using Shuttle Radar Topography Mission data and the Global Multi-resolution Terrain Elevation Data along with other multi-source digital elevation model (DEM) data. A global database of maximum terrain fluctuation with a grid size of $0.05^\circ \times 0.05^\circ$ and distances of 140 and 700 m was then constructed on the basis of the ICESat-2 satellite flight path and the main frame/super frame distance criterion. The databases, which achieve global coverage while occupying a small storage space, can be used to assist in the in-orbit preprocessing of onboard data. The database accuracy was evaluated using ICESat-2 data. In the 10 validation areas, the global DEM database had an error of only 3 m in two validation areas, and the error was less than the accuracy range of each DEM data source. The global terrain database can characterize the degree of surface relief in each verification area, confirming the effectiveness of the method used in this study.

1. Introduction

Elevation databases [digital elevation models (DEMs)] and terrain relief databases [digital relief models (DRMs)] provide essential data that reflect elevation and its variation.⁽¹⁾ Low-resolution global DEM and DRM databases with grid sizes of $0.05^\circ \times 0.05^\circ$ occupy minimal storage space. These lightweight foundational spatial databases meet the requirements of various on-orbit preprocessing algorithms for satellite data.

Common publicly available DEM data such as AW3D30⁽²⁾ and ASTER GDEM⁽³⁾ data (resolution = 30 m) along with Shuttle Radar Topography Mission (SRTM)⁽⁴⁾ and TanDEM-X⁽⁵⁾

*Corresponding author: e-mail: wangjiayu0215@163.com
<https://doi.org/10.18494/SAM5344>

data (resolution = 90 m) have resolutions that are higher than the required grid size of the database. Therefore, further processing of the original DEM data is necessary to meet the grid size requirements. He *et al.*⁽⁶⁾ used data from domestic high-resolution satellites and ASTER GDEM to interpret the status of glacial lakes at a scale of 1:50,000. They extracted terrain relief features using the optimal mean breakpoint method and conducted correlation analysis to assess the hazard level of glacial lake outburst flooding. Feng *et al.*⁽⁷⁾ used ASTER GDEM terrain data to develop the first 30-m terrain relief map of the Qinghai-Tibet Plateau. The authors analyzed the relationship between relief, altitude, and relative elevation difference and defined the effective representation of terrain relief for regional terrain conditions. You *et al.*⁽⁸⁾ used DEM data and, on the basis of the definition and calculation formula of terrain relief under the context of China's livable environment evaluation, used ArcGIS spatial analysis functions to calculate 1 km datasets of terrain relief for China and different administrative units. Although these terrain relief data effectively represent regional terrain conditions, they do not specifically address satellite flight trajectories or meet the requirements for global coverage at a specified grid size.

Against this background, we constructed a global maximum/minimum elevation database with a grid size of $0.05^\circ \times 0.05^\circ$ based on multisource, publicly available DEM data. Additionally, we utilized satellite laser altimetry data, encompassing satellite flight paths and measurements of primary and super frame distances, to establish a comprehensive global database that captures the nuances of terrain relief. These databases provide support for setting the distance window when selecting original photon data from satellite laser altimetry.

2. Data Sources

The global DEM and DRM databases were constructed on the basis of existing publicly available DEM data. Currently, no single data source meets the requirements for global coverage, resolution, and accuracy simultaneously. In this study, we selected six of the best available DEMs for different regions from the existing public DEM data to construct the global database. The selected data sources and their coverage areas are shown in Fig. 1, and the parameters of each data source are listed in Table 1.

SRTM was jointly developed by the National Aeronautics and Space Administration, National Imagery and Mapping Agency, and German and Italian space agencies.⁽⁴⁾ Owing to the limitations of radar instruments and the gaps in data for mountainous and desert regions, the global dataset includes numerous voids. Various organizations have developed algorithms to fill these gaps; for example, CGIAR-CSI provides an SRTM elevation dataset with filled voids and a 3-arcsecond resolution.⁽⁹⁾ In this study, we used SRTM-CGIAR as the data source for land between 60°S and 60°N , with data sourced from the CGIAR's Geospatial Strategy website (<https://csidotinfo.wordpress.com/data/srtm-90m-digital-elevation-database-v4-1>).

The Global Multi-resolution Terrain Elevation Data 2010 (GMTED 2010) was developed by the United States Geological Survey (USGS) and the National Geospatial-Intelligence Agency. This database provides resolutions of 30, 15, and 7.5 arcsec and includes seven raster elevation products (minimum, maximum, mean, and median elevation, elevation standard deviation, systematic statistical sampling, and enhanced feature curvature).⁽¹⁰⁾ Most of these products

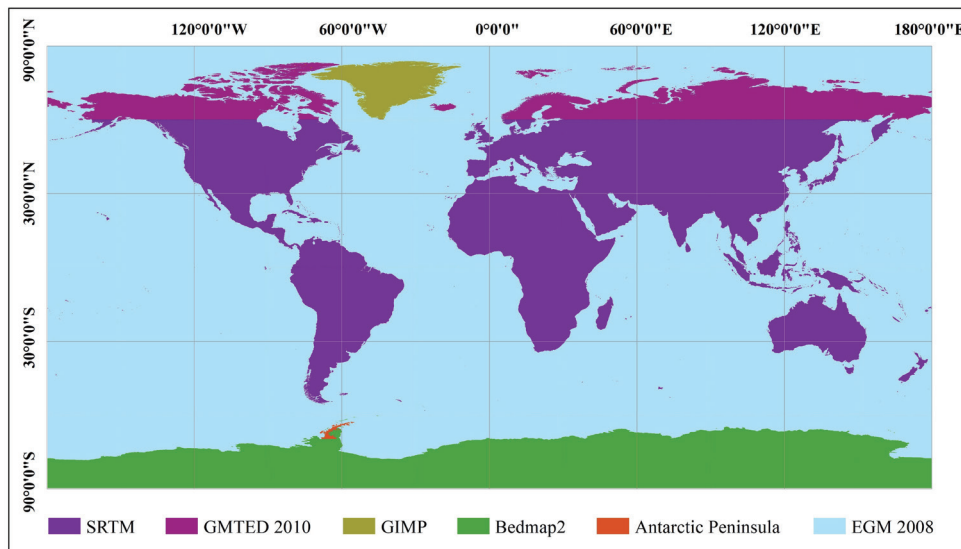


Fig. 1. (Color online) DEM data sources and coverage areas.

Table 1

Parameters of DEM data sources.

Data source	Horizontal datum	Vertical datum	Resolution	Theoretical accuracy
SRTM	GCS WGS 1984	EGM 96 geoid	90 m	±10 m
GMTED 2010	GCS WGS 1984	EGM 96 geoid	250 m	±30 m
GIMP	Polar stereographic	WGS 84 ellipsoid	90 m	±10 m for most regions; ±30 m in mountainous areas
Bedmap2	WGS 1984 antarctic polar stereographic	GL04C geoid	1000 m	±30 m for most ice sheets; ±130 m in mountainous areas
Antarctic Peninsula	WGS 1984 stereographic south pole	EGM 96 geoid	100 m	±25 m

cover all land areas from 56°S to 84°N, while a few cover 90°S to 84°N. In this study, GMTED 2010 was used as the data source for land north of 60°N (excluding Greenland), with data sourced from the USGS website (<https://earthexplorer.usgs.gov>).

The Greenland Ice Mapping Project (GIMP) dataset combines existing elevation products, with ASTER and SPOT-5 data covering the periphery and edge of the ice sheet and Advanced Very High Resolution Radiometer data covering the interior and northern areas of the ice sheet; the data are horizontally and vertically registered using averaged ICESat data. GIMP served as the data source for the Greenland region, with data sourced from the National Snow and Ice Data Center (<https://nsidc.org/data/nsidc-0645/versions/1>).

Bedmap2 integrates laser satellite altimetry data, ice radar sounding data, and satellite remote sensing data into a database of ice sheet and subglacial topography in the Antarctic region. Bedmap2 includes three types of raster data: ice surface elevation, ice thickness, and subglacial bedrock elevation.⁽¹¹⁾ In this study, Bedmap2 was the data source for land south of

60°S, with data sourced from the British Antarctic Survey website (<https://secure.antarctica.ac.uk/data/bedmap2>).⁽¹²⁾

The Antarctic Peninsula DEM dataset is a 100-m-resolution DEM of the surface topography of the Antarctic Peninsula, constructed using ASTER GDEM data. Owing to the relatively low resolution of Bedmap2 data, we used the Antarctic Peninsula DEM as the data source for the region covered by the Antarctic Peninsula, with data sourced from the U.S. Antarctic Program Data Center (<https://www.usap-dc.org/view/dataset/609516>).

The EGM2008 geoid height model was used as the source of elevation data for global ocean areas, with data sourced from the National Geospatial-Intelligence Agency (<https://earth-info.nga.mil>). To distinguish between ocean and land areas, we used the Global Self-consistent, Hierarchical, High-resolution Geography (GSHHG) database released by the University of Hawaii (<http://www.soest.hawaii.edu/wessel/gshhg>) as the boundary between ocean and land.

3. Methodology

The horizontal and vertical data vary among the publicly available DEM data sources. To unify the reference system, the horizontal datum for each DEM was converted to the WGS 84 geographic coordinate system, and the vertical datum was converted to the WGS 84 ellipsoid.⁽¹³⁾ Subsequently, the global DEM and DRM databases were constructed separately. The construction of the DEM database involved setting grid buffers, processing coastal areas, and adjusting anomalous data. In addition to buffer setting, the construction of the DRM database required raster projection and pixel-by-pixel terrain relief calculation. The technical workflow of this study is illustrated in Fig. 2.

3.1 Grid partitioning and buffer zone setting

Using the point (180°W, 90°S) as the origin and with a grid spacing of 0.05° for both longitude and latitude, we divided the global region into a total of 25,920,000 grids. However, owing to positional errors in spaceborne LiDAR footprints, the actual geographic coordinates of LiDAR footprints may fall on the edges of grids, causing their coordinates to lie in adjacent grids based on sensor positioning.⁽¹⁴⁾ Therefore, a 2 km buffer zone was established around each grid to replace the grid area for calculating maximum and minimum elevations as well as maximum terrain relief. As shown in Fig. 3, the inner black box represents the 0.05° × 0.05° grid area, and the outer black box represents the grid area after the addition of the 2 km buffer zone.

When calculating distances between longitudes and latitudes on Earth, it is crucial to consider Earth's ellipsoidal shape and the great circle distance between points on its surface.⁽¹⁵⁾ Flat geometric distance formulas cannot be simply applied in this type of distance calculation because Earth's curvature and ellipsoidal shape mean that distances between longitudes and latitudes are not uniform across different latitudes. Therefore, a more accurate method is necessary to compute the additional longitude and latitude buffers required for the 2 km buffer zone of each grid.

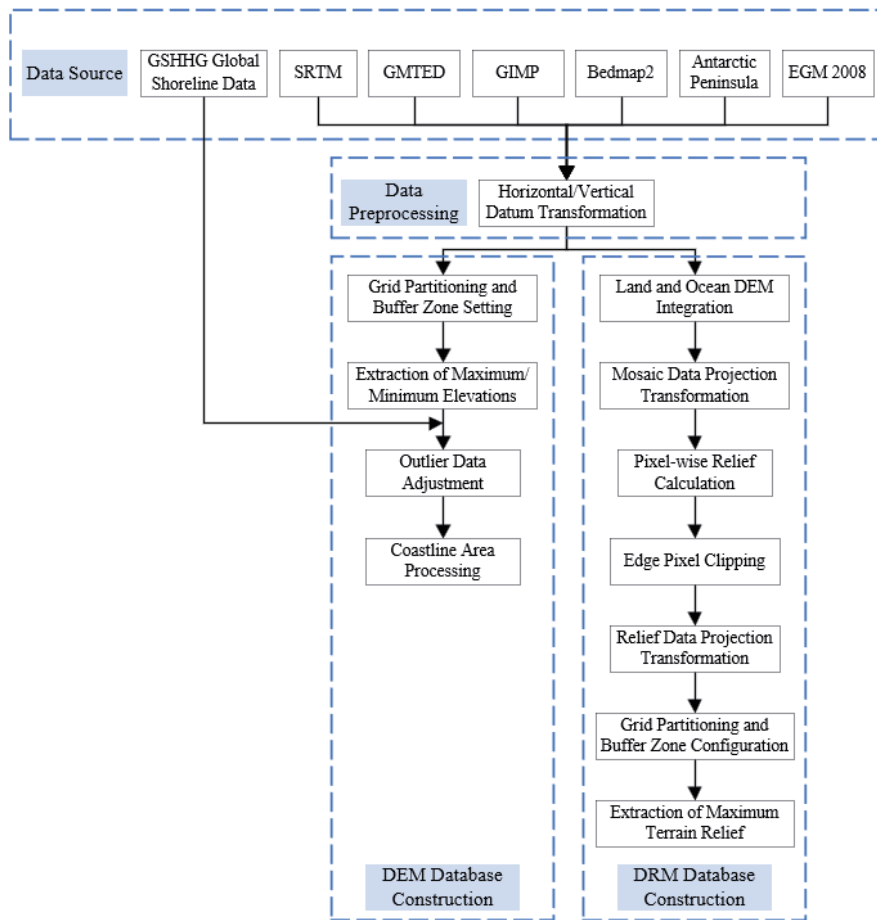


Fig. 2. (Color online) Technical workflow of this study.

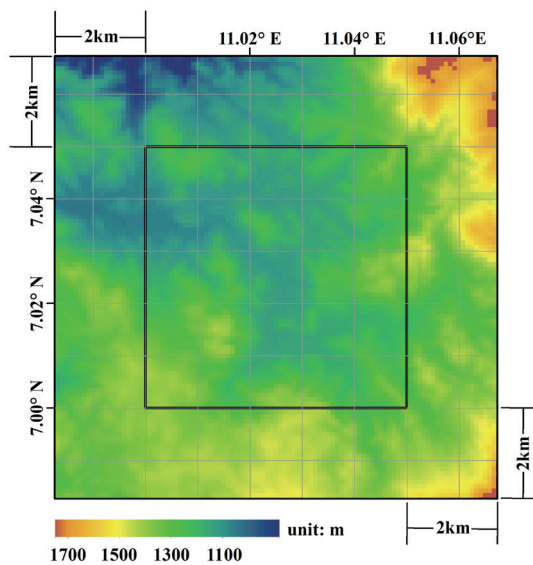


Fig. 3. (Color online) Grid buffer zone setup

In the Python development environment, the “geographiclib” library provides the “Geodesic” class function, which calculates the geographic coordinates of a destination point from a given starting point based on the ellipsoidal model of Earth, great circle distances, and the Vincenty formula.

To determine the longitude and latitude ranges of each grid after adding the buffer, the theoretical longitude and latitude of the grid’s center were used to calculate the buffer zone longitude and latitude. This resulted in the actual longitude and latitude range of the grid after the buffer was added, as shown in the following formula:

$$\begin{cases} lon_max_{actual} = lon_max_{grid} + lon_{buffer} \\ lon_min_{actual} = lon_min_{grid} - lon_{buffer} \\ lat_max_{actual} = lat_max_{grid} + lat_{buffer} \\ lat_min_{actual} = lat_min_{grid} - lat_{buffer} \end{cases}, \quad (1)$$

where lon_max_{actual} , lon_min_{actual} , lat_max_{actual} , and lat_min_{actual} represent the actual maximum longitude, actual minimum longitude, actual maximum latitude, and actual minimum latitude of the grid, respectively; lon_max_{grid} , lon_min_{grid} , lon_min_{grid} , lat_max_{grid} , and lat_min_{grid} represent the theoretical maximum longitude, theoretical minimum longitude, theoretical maximum latitude, and theoretical minimum latitude of the grid, respectively; and lon_{buffer} and lat_{buffer} represent the buffer longitude and buffer latitude of the grid, respectively.

3.2 DEM database construction

3.2.1 Extraction of maximum/minimum elevations

Conventional DEM data pixels represent the average elevation within the pixel area.⁽¹⁶⁾ However, because the pixel size of the DEM database in this study was $0.05^\circ \times 0.05^\circ$, the average elevation within the pixel area cannot adequately represent the elevation information of the region and has no practical significance. Therefore, we constructed global DEM data for both maximum and minimum elevations, which together form the global DEM database.

The maximum and minimum elevations of a grid were respectively defined as the maximum and minimum elevations within the original DEM data source after overlaying the buffer zone onto the grid. As shown in Fig. 4, the maximum elevation within the grid (99.95°E–100.00°E, 40.00°N–40.05°N) was 1570 m and the minimum elevation was 1304 m; these values were incorporated as the maximum and minimum values in the global DEM database, respectively.

3.2.2 Adjustment of outlier data and coastline area processing

Although the SRTM-CGIAR is a version of the SRTM with gaps filled, it still contains data gaps in large inland water bodies (e.g., the Caspian Sea). For these gaps, the EGM 2008 data were integrated with the DEM data, allowing the extraction of the maximum and minimum

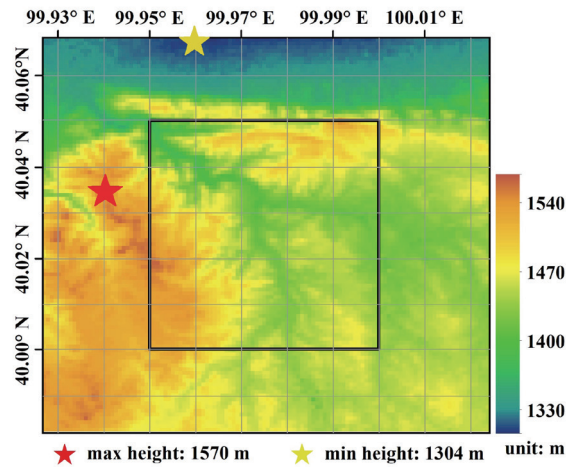


Fig. 4. (Color online) Extraction of maximum and minimum elevations in a grid.

elevations within the grid range of the mosaicked image. As shown in Fig. 5, this method addressed the data gaps in the Caspian Sea region and produced a mosaicked result.

In the SRTM-CGIAR data, pixels beyond land are marked with “No Data” values. The common values used to store “No Data” include -9999 and ± 32768 . When calculating the maximum and minimum elevations for grids, these “No Data” values can skew the results. Therefore, in such grids, the second highest or second lowest elevation was respectively used as the maximum or minimum elevation of the grid.

The DEM data source for oceanic regions was EGM 2008, which differs from the data source used for terrestrial regions. For coastal grids containing both land and ocean parts, further processing was required. Using GSHHG global shoreline data, we determined the distribution of land and ocean in each grid, and the grids were categorized into three types: land, ocean, and coastline. For grids marked as coastline, the maximum and minimum elevations obtained from the land DEM data were compared with those from the ocean EGM 2008 data. The higher of the two maximum elevation values was taken as the final maximum elevation of the grid, while the lower of the two minimum elevation values was taken as the final minimum elevation.

3.3 DRM database construction

Conventional DRM data are composed of slope values within a grid. In the context of this study, with grid sizes of $0.05^\circ \times 0.05^\circ$, the maximum slope value within each grid cannot accurately represent the terrain relief of the region owing to the large coverage area. Therefore, we developed a method based on satellite flight trajectories and specific flight distances to characterize relief. This method is tailored for the applications of spaceborne laser altimetry satellites.

Taking the major frame and super frame of the ICESat-2 satellite, which correspond to distances of 140 and 700 m, respectively, as examples of specific flight distances, the terrain relief within a 140 m flight distance along a flight path is illustrated in Fig. 6. In Fig. 6, the red-

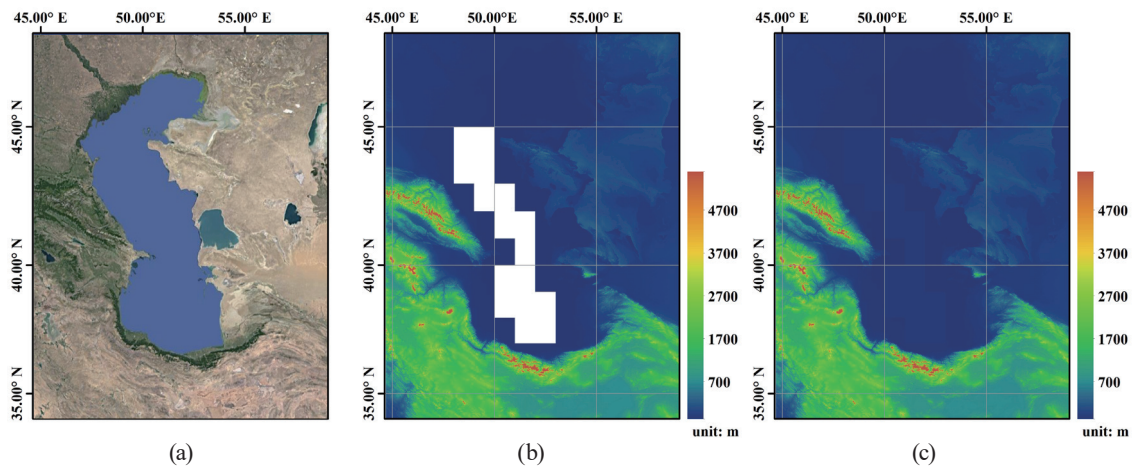


Fig. 5. (Color online) Comparison of DEM data before and after mosaicking. (a) Caspian Sea Google imagery, (b) DEM data before mosaicking, and (c) DEM data after mosaicking.

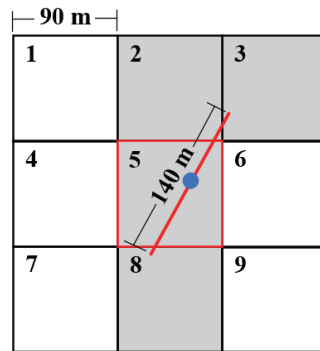


Fig. 6. (Color online) Terrain relief calculation method.

bordered pixel (labeled pixel number 5) is the target pixel, and the red line segment represents a 140 m flight path segment centered within the target pixel. The relief of the target pixel for this flight path segment was defined as the maximum elevation difference among all the pixels traversed by the segment (specifically the difference between the maximum and minimum elevations among the light gray-shaded pixels labeled 2, 3, 5, and 8).

In DRM-140, the maximum terrain relief of the target pixel is determined by the maximum elevation difference among all pixels traversed by 140 m flight path segments centered within the target pixel. In contrast, DRM-700 considers the maximum elevation difference among pixels traversed by 700 m flight path segments.

3.3.1 Pixel-wise relief calculation

Figure 7 shows the flight trajectory of the ICESat-2 satellite. However, modern satellites often have specific maneuvering requirements to complete designated tasks, making it

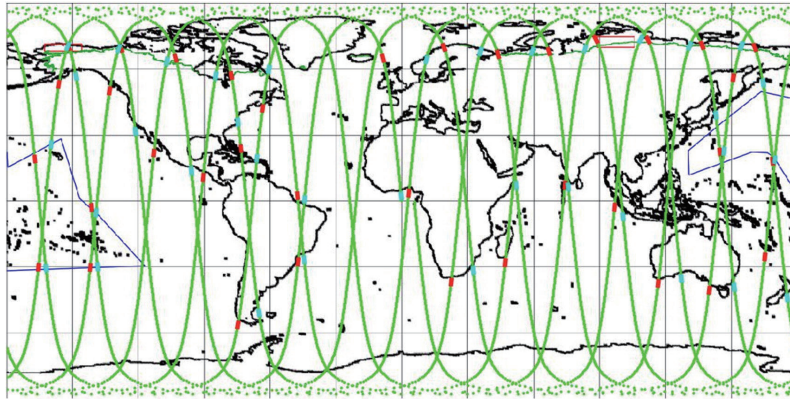


Fig. 7. (Color online) ICESat-2 satellite flight trajectory.⁽¹⁸⁾

challenging to represent the satellite's flight trajectory over its entire lifecycle with a precise flight path.⁽¹⁷⁾ To cover all possible scenarios, the satellite was assumed to be able to fly in any direction within the target pixel. On the basis of this assumption, combinations of pixels that might be traversed during flight distances of 140 and 700 m in DEM data sources with four different resolutions were constructed.

Figure 8 shows the pixel combinations that might be crossed by DRM-140 at DEM resolutions of 90, 100, 250, and 1000 m. Figure 9 shows the pixel combinations that might be crossed by DRM-700 at the same resolutions. In Figs. 8 and 9, the central red-bordered pixel is the target pixel to be processed, and the area covered by the red dashed lines represents the potential paths of 140 m/700 m flight distances centered within the target pixel. The light gray-shaded pixels represent all possible pixels that the flight paths might traverse.

On the basis of the pixel combinations traversed, the pixel-wise difference between the maximum and minimum values among the surrounding pixels of the target pixel was calculated. This difference represents the terrain relief for that pixel. This process yielded DRM data at spatial resolutions of 140 and 700 m, consistent with the original DEM data source. Figure 10 illustrates the DRM-140 data, DRM-700 data, and the corresponding original DEM data for a local region, providing a visual comparison of terrain relief characteristics at different spatial resolutions.

When calculating pixel-wise terrain relief, the high latitudes of regions beyond 60°S or 60°N introduce significant distortions in geographic projection.⁽¹⁹⁾ These distortions cause the pixel's vertical length in meters to decrease from the equatorial nominal resolution to 0 m at the poles due to the cosine of the latitude. Therefore, before calculating pixel-wise terrain relief in high-latitude regions, it was necessary to transform the DEM data from their original coordinate system to a polar stereographic projection. After processing each pixel, the results were transformed back to the WGS84 geographic coordinate system. Additionally, because the pixel-wise calculation of terrain relief relied on surrounding pixels (1/2/4 rings), the edge pixels lacked sufficient neighboring pixels for calculation and were clipped or discarded.

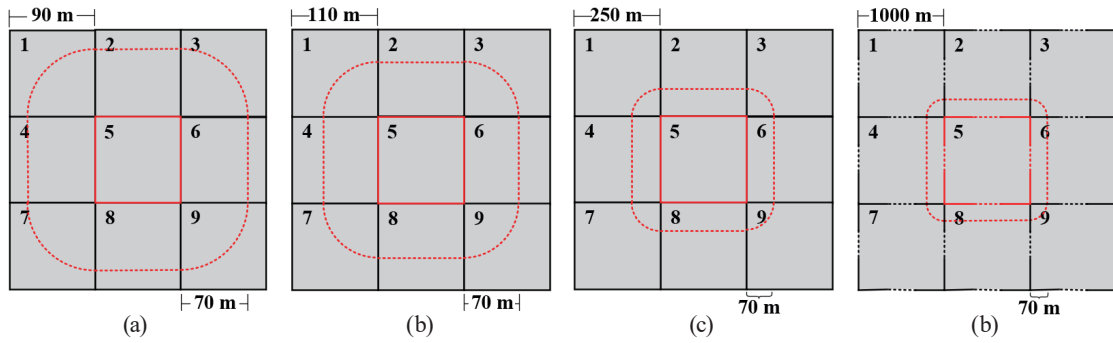


Fig. 8. (Color online) Pixel combinations for DRM-140 m. Resolution = (a) 90, (b) 110, (c) 250, and (d) 1000 m.

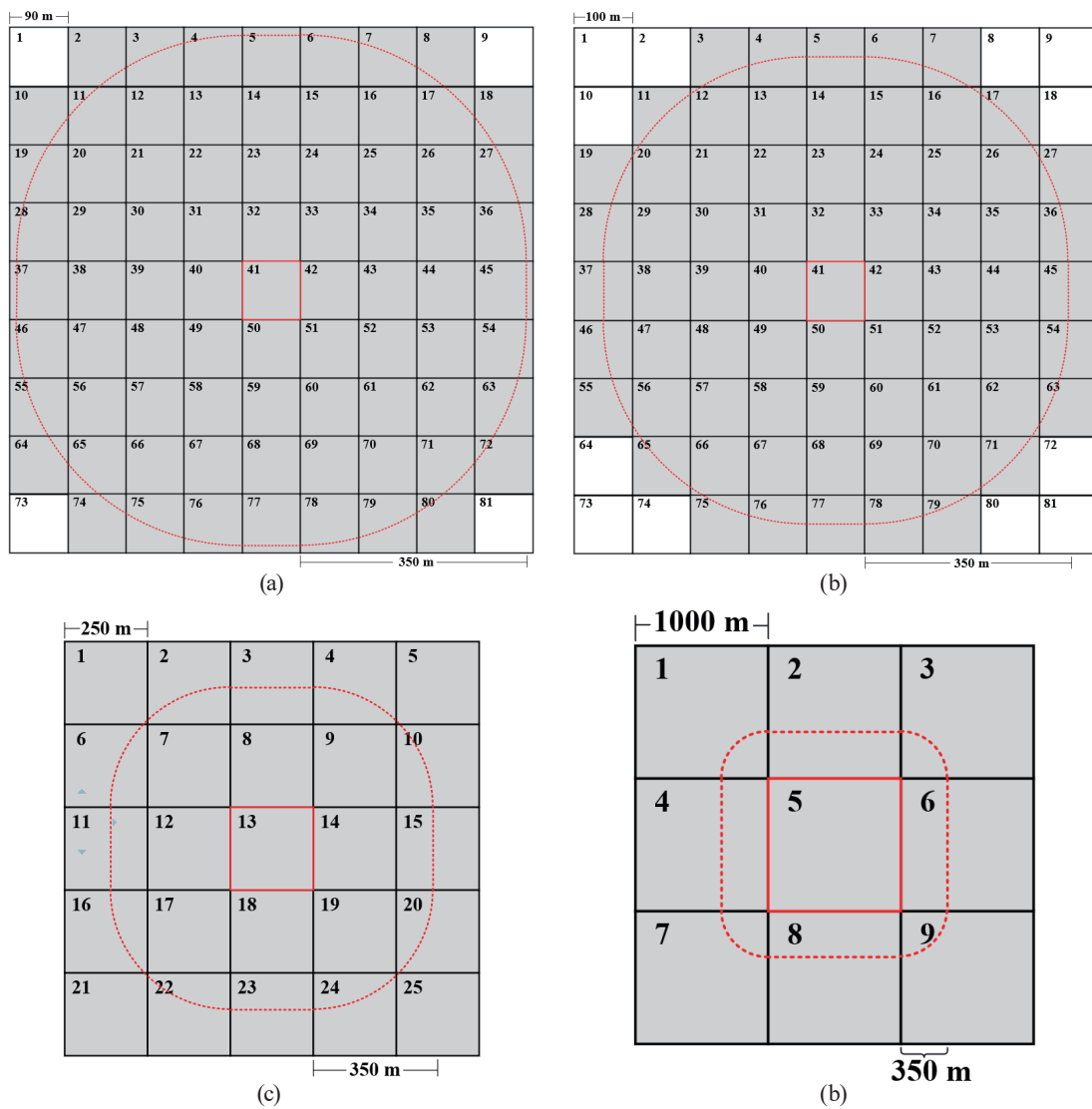


Fig. 9. (Color online) Pixel combinations for DRM-700 m. Resolution = (a) 90, (b) 110, (c) 250, and (d) 1000 m.

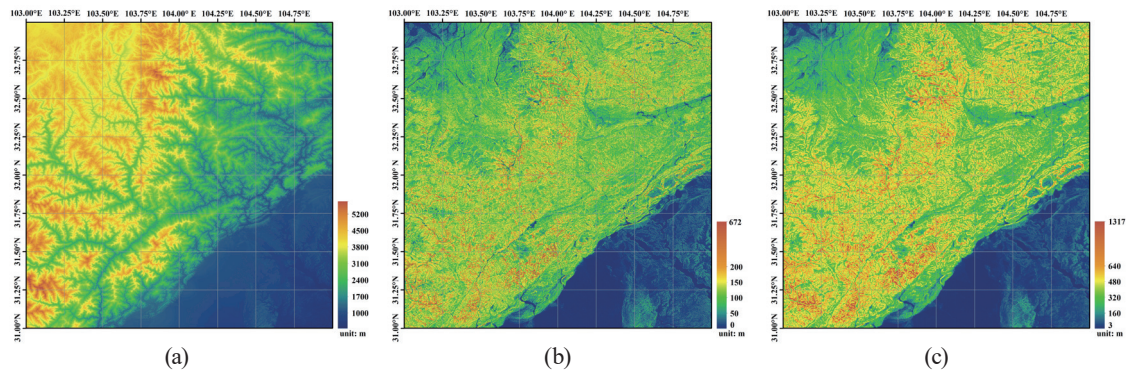


Fig. 10. (Color online) Original DEM data along with DRM-140 and DRM-700 data at the same resolution. (a) Original DEM data, (b) DRM-140, and (c) DRM-700.

3.3.2 DRM construction

Prior to calculating pixel-wise terrain relief, it was necessary to mosaic the land and ocean DEM data such that the resolution of the mosaicked image matched that of the land DEM data source. On the mosaicked images, the pixel-wise terrain relief values were calculated at distances of 140 and 700 m.

On the basis of the grid partitioning and buffer zone settings described in Sect. 3.1, we calculated the terrain relief values for each pixel at distances of 140 and 700 m within the grid boundaries. The maximum value was taken as the maximum terrain relief within the grid.

4. Results and Discussion

4.1 Database results

4.1.1 Global DEM database results

The results of the global DEM database are depicted in Figs. 11 and 12, which show the global DEM minimum and maximum elevation data, respectively.

4.1.2 Global DRM database results

The results of the global DRM database are illustrated in Figs. 13 and 14, which depict the global DRM data at resolutions of 140 and 700 m, respectively.

4.2 Database accuracy assessment

The database accuracy was verified using ICESat-2/ATL08 data. Accuracy validation areas were selected globally on the basis of different surface relief and surface types, including the following:

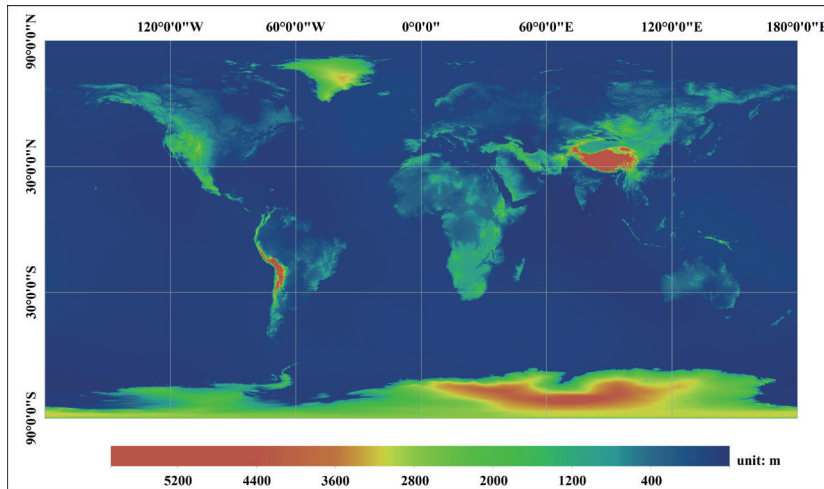


Fig. 11. (Color online) Global DEM minimum elevation data.

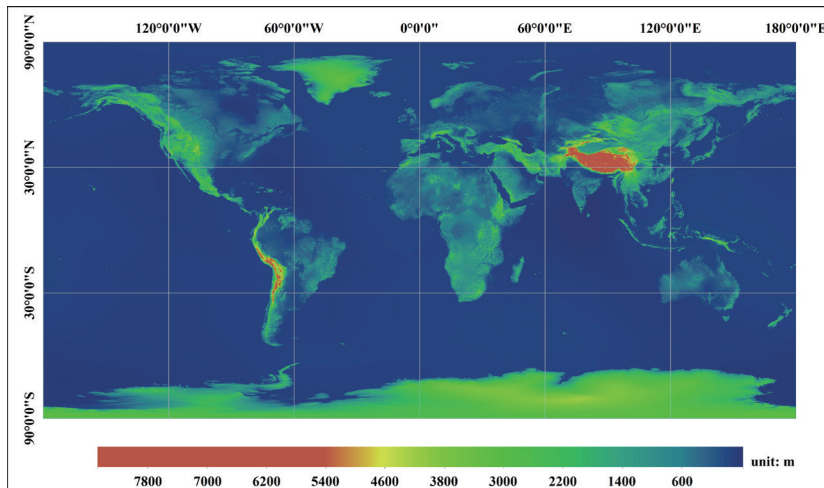


Fig. 12. (Color online) Global DEM maximum elevation data.

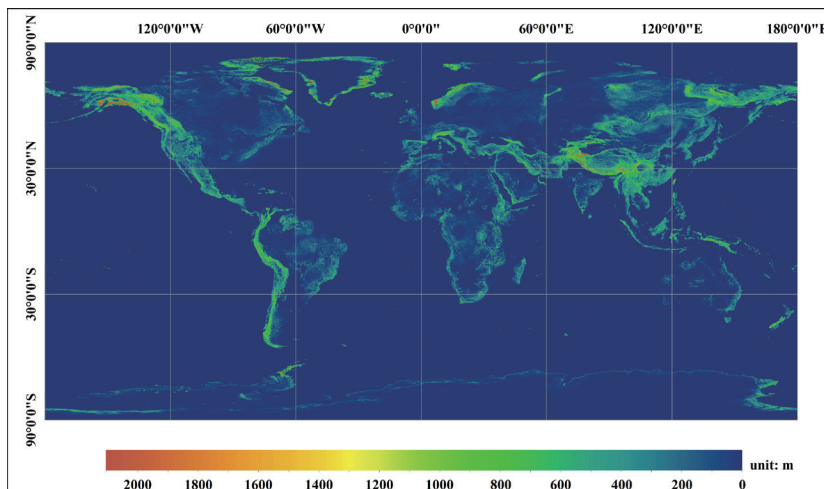


Fig. 13. (Color online) Global DRM data at 140 m resolution.

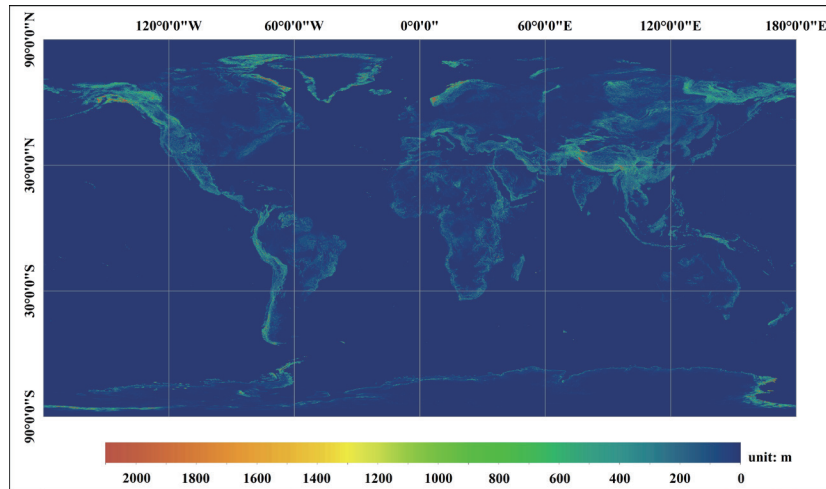


Fig. 14. (Color online) Global DRM data at 700 m resolution.

- High mountains (Qinghai-Tibet Plateau, Huashan, Logan Mountains, and Andes Mountains)
- Polar regions (Antarctica and Arctic)
- Inland water (Lake Ubosu)
- Ocean (Pacific Ocean)
- Forest (Greater Khingan Range)
- Coastline (Hainan)

Detailed information for each validation area is provided in Table 2, and their geographic locations are illustrated in Fig. 15.

Considering the difference in background noise, both daytime and nighttime laser data were collected in the validation areas for verification. Detailed information on the experimental data is provided in Table 3.

4.2.1 Global DEM database accuracy assessment

The maximum and minimum elevations obtained from the ICESat-2 data in each validation area were statistically compared with the maximum and minimum elevations in the corresponding grids of the global DEM database. The results are shown in Table 4 and Fig. 16.

The maximum DEM elevation for Lake Ubosu was 3 m less than the actual maximum elevation measured by ICESat-2, and the minimum elevation in the Pacific validation area was 3 m less than the actual minimum elevation measured by ICESat-2. In all other validation areas, the actual maximum and minimum elevations measured by ICESat-2 fell within the range of the maximum and minimum elevations of the DEM grid.

The validation results demonstrated that the global DEM database constructed in this study accurately represents the actual maximum and minimum elevations within the validation areas. The absolute error exceeded 3 m in only a few validation areas. These discrepancies were observed in water bodies and attributed to changes in water level. These errors might also be related to the accuracy of the original DEM data sources; all discrepancies were smaller than the

Table 2
Details of validation areas.

Validation area	Validation area type	Description
Qinghai-Tibet Plateau	High mountains	Significant terrain relief with maximum elevation differences up to 4000 m. Surface types include bare ground, ice and snow, and sparse vegetation.
Huashan		
Logan Mountains		
Andes Mountains		
Greater Khingan Range	Forest	Relatively flat terrain with dense vegetation
Antarctic Ice Sheet	Ice/Snow	Generally flat terrain with smooth surface covered mainly by ice and snow
Arctic Glaciers		
Lake Uobosu	Water body	Extremely flat terrain
Pacific Ocean		
Hainan	Coastal	Generally flat terrain over the sea, significant elevation variations on land, and dramatic terrain changes at the coastline with distinct surface type differences



Fig. 15. (Color online) Geographic locations of validation areas.

Table 3
Experimental data information.

Validation area	Track ID	Beam	Day/Night
Qinghai-Tibet Plateau	ATL08_20181029092855_04700102_005_01	gt1l	Day
Huashan	ATL08_20200217084038_08040602_005_01	gt1r	Day
Logan Mountains	ATL08_20191012194328_02430505_005_01	gt1r	Day
Andes Mountains	ATL08_20200829115529_09940814_005_01	gt3l	Day
Greater Khingan Range	ATL08_20191001023101_00640506_005_01	gt1r	Day
Antarctic Ice Sheet	ATL08_20181129221517_09510110_005_01	gt2l	Day
Arctic Glaciers	ATL08_20181031072227_04990105_005_01	gt3r	Night
Lake Uobosu	ATL08_20190319140208_12390206_005_01	gt3l	Night
Pacific Ocean	ATL08_20190107112326_01530206_005_01	gt2l	Night
Hainan	ATL08_20200501051222_05450701_005_01	gt1r	Day

Table 4
DEM data accuracy validation results.

Validation area	DEM				ICESat-2		max(DEM) – min(ICESat-2) / m	min(ICESat-2) – min(DEM) / m
	DEM grid range		Max elevation / m	Min elevation / m	Max elevation / m	Min elevation / m		
	Longitude / °	Latitude / °						
Qinghai-Tibet Plateau	79.2/79.25	30.75/30.8	6757	4376	6214	5044	543	668
Huashan	109.95/110	34.45/34.5	2015	365	1651	715	364	350
Logan Mountains	-140.4/-140.35	60.55/60.6	5980	2308	5904	3647	76	1339
Andes Mountains	-76.45/-76.4	-12.55/-12.5	2323	510	2082	1570	241	1060
Greater Khingan Range	125.85/125.9	51.6/51.65	505	288	380	300	125	12
Antarctic Ice Sheet	38.8/38.85	-72.0/-71.95	2503	2429	2494	2460	9	31
Arctic Glaciers	-60.45/-60.4	77.45/77.5	2013	1990	2004	2001	9	11
Lake Ubusu	93.0/93.05	50.3/50.35	713	713	716	716	-3	3
Pacific Ocean	-175.55/-175.5	55.2/55.25	5	4	5	1	0	-3
Hainan	108.85/108.9	19.45/19.5	71	-16	17	-16	54	0

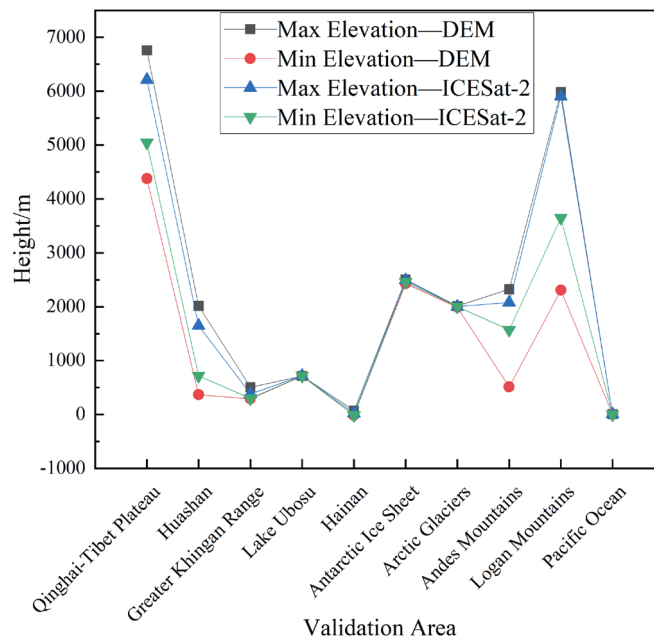


Fig. 16. (Color online) DEM data accuracy validation results.

theoretical errors of the respective DEM data sources listed in Table 1. When using the DEM database to set distance windows for spaceborne laser LiDAR data filtering, a certain buffer distance was added at both ends of the maximum and minimum elevations, further reducing the effect of DEM database errors.

4.2.2 Accuracy assessment of global DRM database

The maximum elevation variations in the ICESat-2 data between distances of 140 and 700 m were calculated in various validation areas. These variations were validated against the DRM-140 and DRM-700 data; the results are shown in Table 5 and Fig. 17.

In the Pacific Ocean validation area, both DRM-140 and DRM-700 showed terrain fluctuations of 0 m, consistent with theoretical expectations of elevation remaining uniform across connected water surfaces. However, the ICESat-2 elevation data indicated a variation of 3 m in terrain relief in this area, possibly due to wave activity on the sea surface or errors inherent in ICESat-2 laser altimetry satellite data. For the remaining nine validation areas, the DRM-140 and DRM-700 values effectively encompassed the maximum terrain fluctuations calculated by ICESat-2 within distances of 140 and 700 m. Additionally, the trends in DRM values across these validation areas closely mirrored those in the ICESat-2 data. These results further validate that the global DRM database presented in this study reasonably and accurately represents surface terrain fluctuations worldwide.

Table 5
DRM data accuracy verification results.

Validation area	DRM				ICESat-2		max(DRM-140) – max(ICESat-2 -140) / m	max(DRM-700) – max(ICESat-2 -700) / m
	DEM grid range		DRM-140 / m	DRM-700 / m	140 m fluctuation / m	700 m fluctuation / m		
	Longitude / °	Latitude / °						
Qinghai-Tibet Plateau	79.2/79.25	30.75/30.8	666	1223	225	690	441	533
Huashan	109.95/110	34.45/34.5	469	751	185	386	284	365
Logan Mountains	-140.4/ -140.35	60.55/60.6	1107	2670	538	1473	569	1197
Andes Mountains	-76.45/ -76.4	-12.55/ -12.5	310	706	68	270	242	436
Greater Khingan Range	125.85/ 125.9	51.6/51.65	114	178	13	40	101	138
Antarctic Ice Sheet	38.8/38.85	-72.0/ -71.95	39	39	1	5	38	34
Arctic Glaciers	-60.45/ -60.4	77.45/77.5	2	4	0	1	2	3
Lake Ubusu	93.0/93.05	50.3/50.35	0	0	0	0	0	0
Pacific Ocean	-175.55/ -175.5	55.2/55.25	0	0	3	3	-3	-3

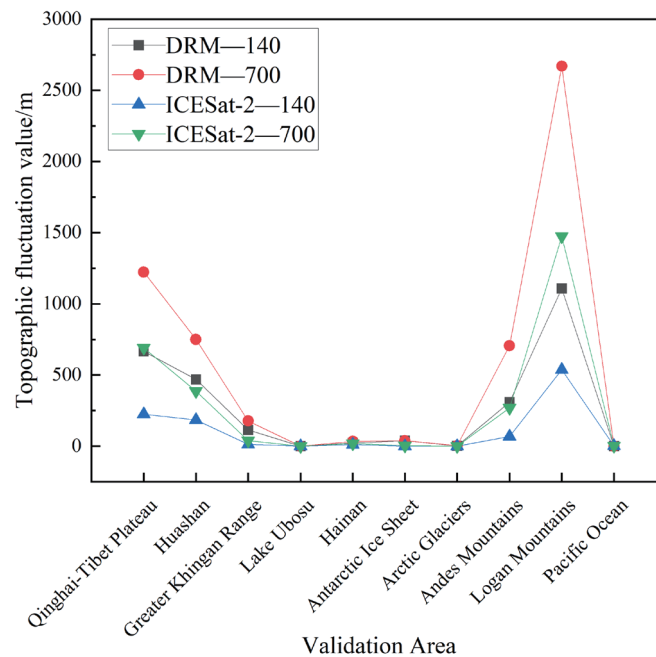


Fig. 17. (Color online) DRM data accuracy verification results.

5. Conclusion

We used publicly available DEM data sources such as SRTM to construct a lightweight global DEM and DRM database with grid sizes of $0.05^\circ \times 0.05^\circ$. To account for horizontal errors in satellite positioning, a 2 km buffer zone was added around each grid. Referring to the primary frame and super frame distances of the ICESat-2 satellite and considering possible satellite flight trajectories, we generated the DRM-140 and DRM-700 databases to capture maximum terrain fluctuations globally between distances of 140 and 700 m.

Validation using ICESat-2/ATL08 data demonstrated that the DEM database constructed in this study accurately represents the elevation range within each grid and that the DRM data effectively characterize surface terrain fluctuations within the grids.

In the future, we plan to incorporate newly released high-resolution DEM datasets to enhance the accuracy and applicability of the database, particularly in complex terrain areas. Additionally, we aim to develop automated update processes to dynamically integrate new data sources, ensuring that the database remains up-to-date and suitable for broader applications, such as environmental monitoring and disaster response.

Acknowledgments

This study was supported by the Independent Innovation Project of Changjiang Survey, Planning, Design and Research Co., Ltd. (ID: CX2023Z31).

References

- 1 H. Yang, Y. Xu, K. Zhou, L. Wang, and L. Xu: *Acta Geogr. Sinica* **78** (2023) 2128. <https://doi.org/10.11821/dlxb202309002>
- 2 T. Tadono, H. Ishida, F. Oda, S. Naito, K. Minakawa, and H. Iwamoto: *ISPRS Annals of the Photogrammetry, Remote Sensing and Spatial Information Sciences*. (ISPRS, 2014) 71–76. <https://isprs-annals.copernicus.org>
- 3 T. Tachikawa, M. Hato, M. Kaku, and A. Iwasaki: *IEEE Int. Geoscience and Remote Sensing Symp.* (IEEE, 2011) 3657-3660. <https://doi.org/10.1109/IGARSS.2011.6050017>
- 4 T. G. Farr, P. A. Rosen, E. Caro, R. Crippen, R. Duren, S. Hensley, M. Kobrick, M. Paller, E. Rodriguez, L. Roth, D. Seal, S. Shaffer, J. Shimada, J. Umland, M. Werner, M. Oskin, D. Burbank, and D. Alsdorf: *Rev. Geophys.* **45** (2007) 2. <https://doi.org/10.1029/2005RG000183>
- 5 P. Rizzoli, M. Martone, C. Gonzalez, C. Wecklich, D. B. Tridon, B. Brutigam, M. Bachmann, D. Schulze, T. Fritz, and M. Huber: *ISPRS J.* **132** (2017). <https://doi.org/10.1109/IGARSS.2011.6050017>
- 6 P. He, L. Tong, Z. Guo, J. Tu, and G. Wang: *Remote Sens. Nat. Resour.* **34** (2022) 1. <https://doi.org/10.6046/zrzyyg.2021065>
- 7 Z. Feng, W. Li, P. Li, and C. Xiao: *Acta Geogr. Sinica* **75** (2020) 7. <https://doi.org/10.11821/dlxb202007003>
- 8 Z. You, Z. Feng, and Y. Yang: *J. Global Change Data Discovery* **2** (2018) 2. <https://doi.org/CNKI:SUN:QQSJ.0.2018-02-005>
- 9 Z. Li, P. Li, D. Ding, and H. Wang: *Geomatics Inf. Sci. Wuhan University* **43** (2018) 12. <https://doi.org/10.13203/j.whugis20180295>
- 10 X. Tang, S. Li, T. Li, Y. Gao, S. Zhang, Q. Chen, and X. Zhang: *J. Remote Sens.* **25** (2021) 1. <https://doi.org/10.11834/jrs.20210210>
- 11 P. Fretwell, H. D. Pritchard, D. G. Vaughan, J. L. Bamber, N. E. Barrand, R. Bell, C. Bianchi, R. G. Bingham, D. D. Blankenship, and G. Casassa: *Cryosphere Discuss.* **7** (2013) 1. <https://doi.org/10.5194/tcd-6-4305-2012>
- 12 G. H. Leonard, S. M. Mager, A. G. Pauling, K. G. Hughes, and I. J. Smith: *J. Spatial Sci.* **59** (2014) 297. <https://doi.org/10.1080/14498596.2014.913271>
- 13 X. Zhu, Z. Ren, S. Nie, G. Bao, G. Ha, M. Bai, and P. Liang: *Remote Sens.* **15** (2023) 1480. <https://doi.org/10.3390/rs15061480>
- 14 Y. Yang, J. Wang, J. Su, C. Yang, and R. Cheng: *Sci. Surv. Mapp.* **48** (2023) 17. <https://doi.org/10.16251/j.cnki.1009-2307.2023.09.003>
- 15 L. I. Baccaro, M. S. Akmentins, C. G. García, and J. J. Martínez: *J. Biogeogr.* **1** (2024) 1560. <https://doi.org/10.1111/jbi.14845>
- 16 Y. Zhou, X. Li, D. Zheng, S. Ren, Y. Wang, and Z. Li: *Acta Geodaetica et Cartographica Sinica* **53** (2024) 779. <https://doi.org/10.11947/j.AGCS.2024.20230260>
- 17 L. Wang, Q. Li, L. Wu, L. Wang, X. Yang, and X. Li: *J. Astronaut.* **45** (2024) 1123.
- 18 T. Markus, T. Neumann, A. Martino, W. Abdalati, and K. Brunt: *Remote Sens. Environ.* **190** (2017) 260-273. <https://doi.org/10.1016/j.rse.2016.12.029>
- 19 W. Pan, A. Li, and X. Liu: *Laser & Optoelectron. Prog.* **61** (2024) 1. <https://doi.org/10.3788/LOP241417>